Polymer 51 (2010) 6319–6333

Contents lists available at ScienceDirect

Polymer

journal homepage: www.elsevier.com/locate/polymer

Annealing effect upon chain orientation, crystalline morphology, and polarizability of ultra-thin P(VDF-TrFE) film for nonvolatile polymer memory device

Jong Soon Lee [1], Arun Anand Prabu [2], Kap Jin Kim*

Department of Advanced Materials Engineering for Information and Electronics, College of Engineering, Kyung Hee University, Yongin-si, Gyeonggi-do 446-701, South Korea

ARTICLE INFO

Article history:
Received 15 August 2010
Received in revised form
16 October 2010
Accepted 29 October 2010
Available online 3 November 2010

Keywords:
Ultra-thin P(VDF-TrFE) film
Chain and dipole orientation
Nonvolatile ferroelectric polymer memory

ABSTRACT

The ferroelectric behavior of spin-cast ultra-thin P(VDF-TrFE) (72-28) film is highly influenced by sample preparation methods including thermal annealing. The effect of sample preparation methods on the surface morphology, chain and dipole orientation, ferroelectric properties, and nonvolatile memory characteristics were studied using FTIR-grazing incident reflection absorption spectroscopy (GIRAS), grazing incident wide angle X-ray diffraction (GIWAXD), atomic force microscope (AFM), dynamic contact electrostatic force microscope (DC-EFM), and polarization-electric field (*P-E*) hysteresis measurements to find the feasibility of applying the ultra-thin P(VDF-TrFE) film to scanning probe microscopy (SPM)-based storage device or low-cost nonvolatile ferroelectric polymer random access memory (NvFePoRAM) device. From the collective analysis of GIRAS, GIWAXD, and AFM data, annealing the as-cast sample at temperature (ca. 120 °C) above Curie transition, but below its melting transition temperature was found to be the most suitable condition to fabricate the NvFePoRAM and/or SPM-based storage device with a memory density of about 30 GB/in^2. DC-EFM technique was successfully used to characterize the nonvolatile memory properties by 'writing and erasing' the data bit through applying a dc bias voltage much larger than coercive voltage with different polarities and then reading the data bit by applying a high frequency ac voltage of only 2 V to the 'written or erased' area.

1. Introduction

Since poly(vinylidene fluoride-co-trifluoroethylene) [P(VDF-TrFE)] has a ferroelectric crystal phase showing a hysteresial *P-E* curve like a piezoelectric ceramic material such as PZT below Curie transition temperature (T_c) irrespective of film preparation methods, this ferroelectric polymer is of particular interest for piezoelectric sensor and actuator, pyroelectric sensor, and nonvolatile memory device applications [1–5]. In case of piezoelectric sensor and actuator applications to withstand external mechanical stress and mechanical deformation induced by an applied electric field, about 25–1000 μm thick films produced by melt-processing followed by uniaxial or biaxial stretching are widely used [1] (www.meas-spec.com/piezo.aspx). In the case of memory device applications, however, submicron-thick film is required using melt-processing or solution casting to reduce drastically the programming voltage for data recording or data erasing [4,6–8]. In all cases, better electronic performance is highly related to higher magnitude of remanent polarization (P_r). Since the ferroelectricity of the P(VDF-TrFE) film is originated from the response of CF-dipoles in the ferroelectric crystal phase, not in the amorphous phase, to an external electric field, it is very important to increase the dipole orientation toward the electric field direction as well as the crystallinity so that one may make higher performance electric devices.

The best well-known method to increase the crystallinity of the solution cast or melt-processed P(VDF-TrFE) film sample is well known to anneal it at the temperature between T_c and melting temperature (T_m) [9–11]. The maximum crystallinity, however, does not always yield the maximum P_r remanent polarization after poling at the same electric field. When two types of P(VDF-TrFE) films (one is unoriented and the other is oriented uniaxially (or biaxially)) are assumed to be of exactly same crystallinity, the oriented film shows higher P_r than the unoriented one under the same poling condition. This is because the preferential orientation

* Corresponding author. Tel.: +82 31 201 2518; fax: +82 31 204 8114.
E-mail address: kjkim@khu.ac.kr (K.J. Kim).
[1] Present address: Analytical Research Center, R&D Business Labs, Central Research Institute, Hyosung Corporation, Anyang-si, Gyeonggi-do 431-080, South Korea.
[2] Present address: Department of Chemistry, School of Advanced Sciences, Vellore Institute of Technology University, Vellore 632014, Tamil Nadu, India.

0032-3861/$ – see front matter © 2010 Elsevier Ltd. All rights reserved.
doi:10.1016/j.polymer.2010.10.053

of the *c*-axis of the P(VDF-TrFE) crystal lattice along the oriented film surface can yield greater degree of CF-dipole orientation toward the external electric field direction, since the CF-dipole vector parallel to the *b*-axis is perpendicular to the *c*-axis [12]. That is why the thick P(VDF-TrFE) films used as piezoelectric sensor and actuator are always stretched uniaxially or biaxially before poling.

Ferroelectric memory devices with P(VDF-TrFE) thin films have a variety of device architectures such as metal-ferroelectric-metal (MFM) capacitors [13–15], MF-insulator-semiconductor (MFIS) diodes [5,14,16–19], and comparatively advanced ferroelectric field effect transistor (FeFET) architectures [16,18–21]. Since P(VDF-TrFE) films have a relatively large coercive field (E_c) of approximately 50 MV/m, all of these memory devices require submicron-thick P(VDF-TrFE) films on substrates to be operated with low programming voltage. Submicron-thick film deposition on an appropriate substrate can be made mostly by spin-coating [4,6,10,22], or Langmuir–Blodgett's method [5,7,8]. Although the Langmuir–Blodgett-deposited P(VDF-TrFE) film has several tens of monolayers of extremely high crystallinity and preferential orientation of *c*-axis along the substrate surface, it cannot be applied to the fabrication process of real memory device due to many unresolved problems and very low-cost effectiveness. On the other hand, spin-coating is most widely used because of very simple and cost effective process applicable to very large area devices. Spin-coating process necessarily requires annealing to increase the crystallinity of as-cast film on the substrate for enhancement of electric device performance. When P(VDF-TrFE) (72-28 mol %) copolymer thin films were obtained by spin-coating method, we recently reported a significant increase in the degree of crystallinity for samples annealed at T_c range (110–120 °C) [10], and drastically reduced degree of crystallinity for spin-coated films below their threshold crystallization thickness (<130 nm) [11]. Although, however, this post-annealing also affects chain orientation, crystal lattice orientation, lamellar size, surface topography, electrical properties, etc, there have been very few papers [22,23] investigating systematically all of these properties influenced by various annealing conditions and interrelation with one another.

In this paper, we focused our attentions on investigating the effect of annealing conditions on chain and CF-dipole orientation, surface topography, and nonvolatile memory characteristics using grazing incident reflection absorption Fourier transform infrared spectroscopy (GIRAS), grazing incident wide angle x-ray diffraction (GIWAXD), atomic force microscopy (AFM), dynamic contact electrostatic force microscopy (DC-EFM), and *P-E* hysteresis measurement to find the feasibility of using ultra-thin P(VDF-TrFE) films for nonvolatile ferroelectric polymer memory (NvFePoRAM) or scanning probe microscopy (SPM)-based data storage device.

2. Experimental

2.1. Materials and sample preparation

P(VDF-TrFE) (72–28 mol %) samples in the form of pellets were obtained from Solvay, USA. The P(VDF-TrFE) thin films were prepared as follows. 50–275 nm-thick films were prepared by spin-casting various concentrations of P(VDF-TrFE) solution in MEK with a spin-coater (1500 rpm for 30 s) under N_2 atmosphere on the gold-coated glass and Si-wafer, and ITO glass (used as bottom electrode). Various annealing conditions such as (a) as-cast (AC) at R.T., (b) as-cast and then annealed (AN) above T_c, but below T_m (120 °C, 3 h), (c) melt (200 °C, 10 min)-quenched (MQ), and (d) melt-slowly cooled (−2 °C/min) (MSC) were adopted to see the effect of annealing conditions on various physical and electrical properties of the P(VDF-TrFE) films. The average thickness of films cast on the substrates was measured using an atomic force microscope (AFM, XE-100, PSIA, Korea) at R.T.

2.2. Grazing incident reflection absorption fourier transform infrared spectroscopy (GIRAS)

GIRAS data were collected using a Bruker-IFS66V spectrometer with 300 scans at an incidence angle of ca. 85° from the normal to the surface at a resolution of 2 cm^{-1}. GIRAS measurements were made only for the samples cast on gold-coated glass or Si-wafer substrate.

2.3. Corona poling

The AN, MQ, and MSC samples cast on gold-coated Si-wafer were corona poled under the application of DC voltage of 16 kV for 30 min with a sample-to-tip distance of 3 cm. The degree of CF-dipole orientation toward the electric field direction during poling was evaluated for each sample annealed under different annealing conditions using *in situ* GIRAS data.

2.4. Grazing incident wide angle X-ray diffraction (GIWAXD)

To characterize the crystalline structure and lattice orientation of the samples cast on the gold-coated glass, GIWAXD measurements were performed on the 4C2 beam line in the PAL (Pohang Accelerator Laboratory, Korea) using monochromatic X-ray ($\lambda = 0.1608$ nm) under vacuum and incident angle of 0.32°. The samples were mounted on an *x* and *y* axes goniometer equipped with a hot stage. The diffracted beam intensity was detected with a 2D-CCD detector (SCX:4300-165/2, Princeton Instruments, USA) and saved in a PC for further analysis. 2D-GIWAXD patterns were obtained in the range $0 < q_z < 27.2\ nm^{-1}$ and $-11.1 < q_{xy} < 27.2\ nm^{-1}$ ($q = 4\pi \cdot \sin\theta/\lambda$, z is perpendicular and xy is parallel to the substrate).

2.5. Surface morphology and DC-EFM measurements

To characterize the surface topography of the samples, atomic force microscopic images were obtained on an XE-100 Atomic Force Microscope (AFM, Park Systems Co., Korea) in a non-contact mode using a Si cantilever with a nominal spring constant of 0.2 N/m and a tip radius of about 10 nm in an area of 1×1–$10 \times 10\ \mu m^2$. The ferroelectric response images were obtained using XE-100 (PSIA, Korea) using a cantilever with a conductive Ti–Pt coated tip in a dynamic contact electrostatic force microscopic mode (DC-EFM). Only as-cast annealed (AN) thin films were used in DC-EFM measurement. More detailed experimental setup is described in the text.

2.6. Polarization (P-E) measurement

For measuring the electrical properties, Al electrodes of diameter 200 μm were vacuum-deposited on the top surface of the cast films on the ITO glass under a pressure of $\sim 10^{-6}$ mbar and a rate of 0.1 nm/s. *P-E* measurements were carried out on a ferroelectric tester (Precision LC, Radiant Technologies, USA) using a virtual ground circuit.

3. Results and discussion

3.1. Crystallinity and chain and dipole orientation

Since the ferroelectric crystal structure of P(VDF-TrFE) with the VDF content of greater than 70 mol% is nearly identical to the orthorhombic β-crystal structure of PVDF as seen in the inset of Fig. 1a, CF_2 dipoles are parallel to *b*-axis, and molecular chain is

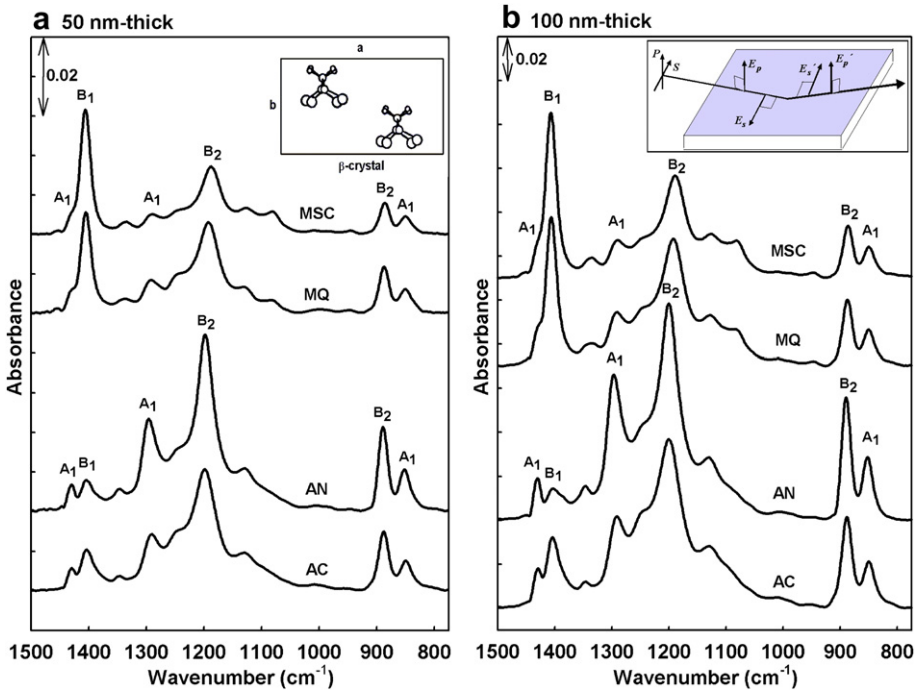

Fig. 1. FTIR-GIRAS spectra measured at room temperature for (a) 50 nm and (b) 100 nm-thick P(VDF-TrFE) films obtained with different preparation methods. Inset (a): unit lattice of P(VDF-TrFE); inset (b): geometry of GIRAS measurement.

along *c*-axis [24,25]. Since FTIR-GIRAS is very sensitive to changes in crystallinity, chain orientation, and dipole orientation in ultra-thin film [10,11,26], this technique was adopted to evaluate the effect of sample preparation methods on changes in crystallinity, chain orientation, and dipole orientation in ultra-thin films. In GIRAS used without a polarizer with the IR incident angle closer to grazing incident angle (ca. 80–88°), only the *p*-polarized component (E_p) of the vibrational mode is enhanced exclusively, whose electric vector is perpendicular to the metal substrate surface [10]. At this angle, it predominantly detects the vibrational modes with the transition moments normal to the substrate surface as seen in the inset of Fig. 1b. Fig. 1 shows the GIRAS spectra of 50 and 100 nm-thick P(VDF-TrFE) films prepared under varying thermal conditions.

Compared to the AC sample, the characteristic bands of *trans*-zigzag conformation of the AN sample, e.g. the 1292 cm^{-1} band (A_1, $\vec{\mu} \parallel \vec{b}$) for the VDF *trans* sequence longer than TTTT, the 848 cm^{-1} band(A_1, $\vec{\mu} \parallel \vec{b}$) for the *trans* sequence longer than TTT, and 1182 and 888 cm^{-1} bands (B_2, $\vec{\mu} \parallel \vec{a}$) associated with crystalline phase show an increase in absorption intensity due to the increased crystallinity upon annealing. The intensity of the 1404 cm^{-1} (B_1, $\vec{\mu} \parallel \vec{c}$) band assigned to ω_{CH_2} coupled with $\nu_{as,C-C}$, in which the transition moment is along the chain direction, was observed to be very weak for both AC and AN samples. From this result, it is worth noting that the molecular chain axis (*c*-axis) of the P(VDF-TrFE) lamellar crystal formed after being spin-coated on the gold substrate is preferentially oriented along the substrate, even though the orientation of the other two axes, *a*- and *b*-axes, is not known. During spin-coating, most of polymer chains can be preferentially oriented along the radial direction of the substrate surface and its orientation can be frozen due to solidification caused by the rapid evaporation of solvent at a very high shear rate generated by high centrifugal force. Therefore, relaxation from the chain extended state to the random coiled state is not allowed even after spin-coating. The absorbance of the 1404 cm^{-1} for the AN sample is observed to be weaker than for the AC sample. This indicates that some random coiled chains present even after spin-casting undergoes thermal relaxation during the annealing treatment resulting in preferential orientation of *trans*-zigzag chains parallel to the substrate surface [6]. Therefore, this kind of thermal annealing results in decreased B_1 intensity along with increased A_1 as well as B_2 crystalline peak intensities.

Fig. 2 shows the absorbances at 1404 cm^{-1} (B_1 band), 1292 cm^{-1} (A_1 band), 888 cm^{-1} (B_2 band), and 848 cm^{-1} (A_1 band) measured at room temperature for 50 and 100 nm-thick P(VDF-TrFE) films prepared under different thermal conditions. From Fig. 2, it is clear that A_1 and B_2 band absorbances of the AN sample are highest and B_1 band absorbance of the AN sample is lowest. The lowest intensity of the chain orientation sensitive B_1 band of the AN sample indicates that the average vibrational transition moment vector of B_1 band is quite close to perpendicular direction of the electric vector of the incident *p*-polarized light (inset of Fig. 1b). Consequently, the *trans*-zigzag chains tend to orient parallel to the substrate surface after annealing treatment. This GIRAS data can be correlated with the uniform film surface observed from AFM images of the AC and AN samples shown later in Figs. 8 and 9. For the MQ and MSC samples, there is a significantly big change in chain orientation as observed from the abrupt increase in the absorbance at 1404 cm^{-1} (B_1 band). This indicates that the chains preferentially oriented along the substrate surface for the AC and AN samples moved quite away from the substrate surface in the course of melt-crystallization. With the preferential chain orientation for the MQ and MSC samples normal to the surface plane, i.e., parallel to the poling direction, it became extremely difficult for the C–F dipoles to switch along the poling direction and hence unsuitable for device fabrication.

The reduced intensity of crystalline A_1 and B_2 bands in the 50 nm-thick film compared to that of the 100 nm-thick sample is due to the sharp decrease in the degree of crystallinity for the 50 nm sample when compared to the 100 nm sample. Xia et al. [22] and Jin et al. [26] have also reported that the final degree of crystallinity was found to be severely affected below the critical

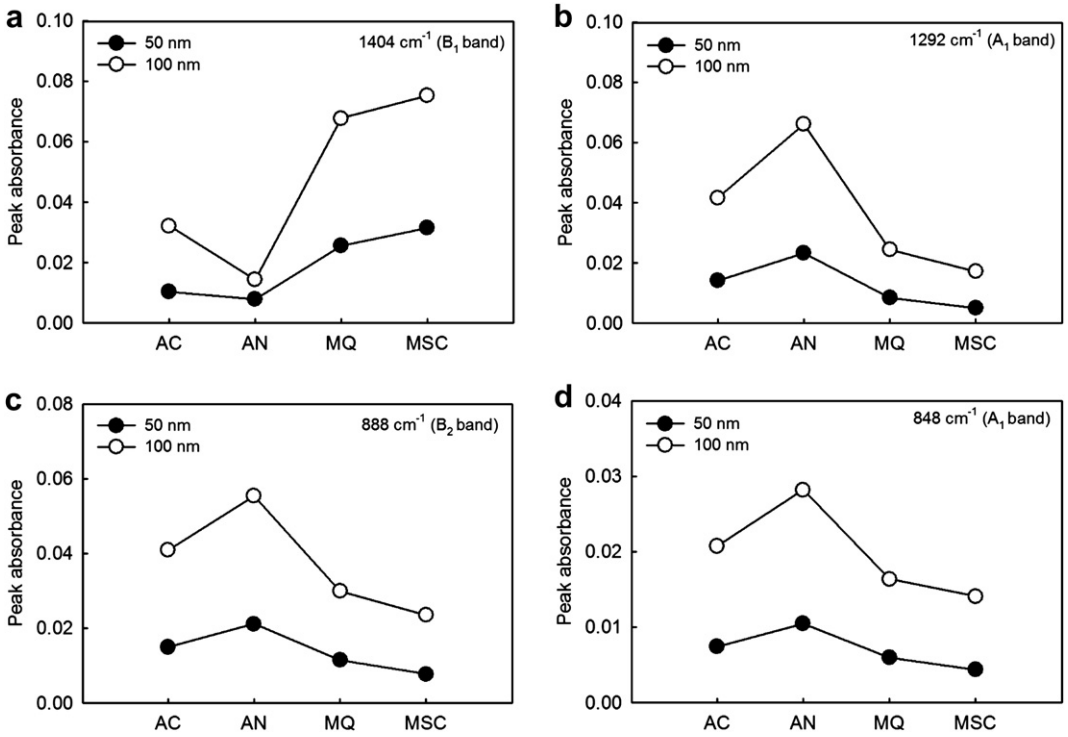

Fig. 2. (a) 1404 cm^{-1}, (b) 1292 cm^{-1}, (c) 888 cm^{-1}, and (d) 848 cm^{-1} band absorbances measured at room temperature for 50 and 100 nm-thick P(VDF-TrFE) films prepared under different thermal conditions.

thickness (<100 nm). Since FTIR-GIRAS is much more sensitive to the changes in crystallinity for nanoscale ultra-thin films, we can clearly observe the significant decrease in A_1 and B_2 bands intensities for the 50 nm-thick film compared to the 100 nm-thick film (in Fig. 2b,c,d).

3.2. GIWAXD analysis

Since GIWAXD was introduced in 1981, it has been often used for evaluating the crystalline structure, crystallinity, chain orientation, and dipole orientation of thin films similar to GIRAS. In this work, the GIWAXD technique was also adopted to evaluate the effect of sample preparation methods on the changes in crystallinity, chain orientation, and dipole orientation in ultra-thin films of P(VDF-TrFE) (72–28) copolymer.

Fig. 3 shows the GIWAXD patterns of the 100 nm-thick P(VDF-TrFE)) film spin-cast on the gold substrate with various thermal treatments. The X-ray diffraction peak of unoriented P(VDF-TrFE) with VDF composition of more than 65 mol% observed at the lowest Bragg angle is indexed as (110)/(200), because the ferroelectric crystal lattice of the P(VDF-TrFE) is of a pseudo-hexagonal orthorhombic lattice with a $\sqrt{3}/1$ ratio of its *a*- and *b*-axes and in turn results in nearly identical (100) and (200) interplanar spacing [24,27]. Thus, for the AN sample in Fig. 3a, the arced strong reflection near $q_z = 14.1$ nm^{-1} with two-fold symmetry on the meridian direction must correspond to (110) and/or (200) reflection of orthorhombic P(VDF-TrFE) crystals. This result also indicates the preferential crystal orientation in which the molecular chain axis (*c*-axis) is preferentially aligned parallel to the substrate surface [6,23] as discussed using GIRAS data in the above section.

If the (200) plane contacts the gold substrate surface dominantly, that is, the *b*-axis is oriented parallel to the substrate surface, the absorption intensity of A_1 bands (1292 and 848 cm^{-1}) must be vanishingly low in the GIRAS of the AN sample. But one can observe the two peaks of medium intensity clearly in the two AN spectra shown in Fig. 1. If the (110) plane contact is dominant, the *b*-axis is oriented at 60° to the substrate surface and the *a*-axis is oriented at 30° to the substrate surface. In this case, since the ratio of vibrational transition moment of the 888 cm^{-1} peak to that of the 848 cm^{-1} peak is 1.23:1 from the IR spectrum of randomly oriented P(VDF-TrFE) film and the angles these two transition moments are making with the electric vector of *p*-polarization IR in GIRAS geometry are approximately 60° and 30°, respectively, the resultant absorption intensity ratio of the 888 cm^{-1} peak to the 848 cm^{-1} peak ($1.23^2 \times \cos^2 60°:1^2 \times \cos^2 30°$) will be approximately 0.5:1, i.e., the absorbance of the 848 cm^{-1} peak must be two times greater than that of the 888 cm^{-1} peak. This is not the case (ca. 1.89:1 from GIRAS spectrum of the 100 nm-thick AN film). Therefore, the AN sample must have the mixture of the (200) and (110) contacts to the substrate with the preferential orientation of the *c*-axis along the substrate surface. From the intensity ratio of the 888 cm^{-1} peak to the 848 cm^{-1} peak (ca. 1.89:1) and the intrinsic ratio of vibrational transition moment of the 888 cm^{-1} peak to that of the 848 cm^{-1} peak (ca. 1.23:1), the average angles that the transition moment of the 888 cm^{-1} peak, i.e., *a*-axis, and the transition moment of the 848 cm^{-1} peak, i.e., *b*-axis, are making with the *p*-polarization IR vector (nearly same as the substrate surface normal) could be calculated as 41.8° and 48.2°, respectively.

For the MQ sample in Fig. 3b, a very strong diffraction arc corresponding to both (110) and (200) was observed newly at $q = 14.1$ nm^{-1} on the azimuthal angle of 60°, whereas the meridional diffraction arc became extremely weak. For the MSC sample in Fig. 3c, the arced strong reflection corresponding to both (110) and (200) was observed only around azimuthal angle of 60°. This reveals that the *c*-axis is not preferentially oriented along the substrate surface any longer after melt-quenching and slowly cooling from the melt. If the molecular chain axis, i.e., *c*-axis, is

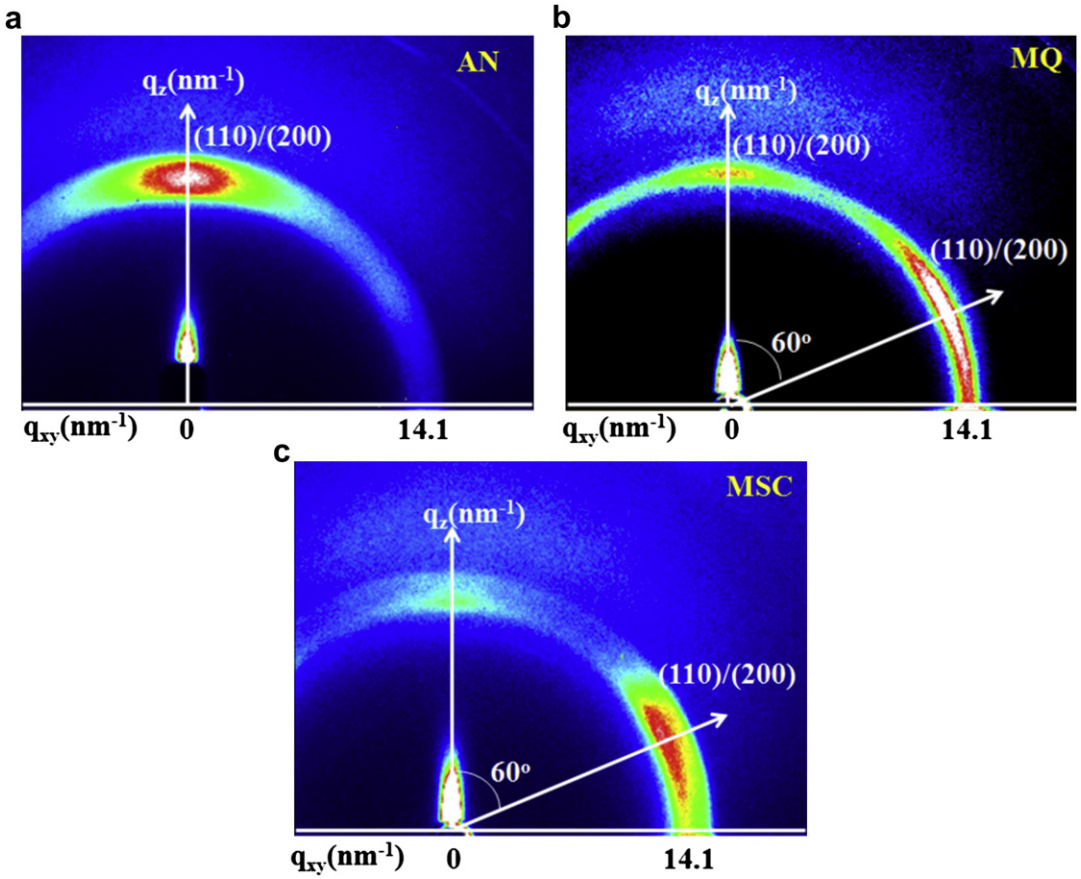

Fig. 3. GIWAXD patterns of the 100 nm-thick P(VDF-TrFE) film spin-cast on the gold substrate with various thermal treatments.

aligned normal to the surface direction, which in turn results in both *a*- and *b*-axes parallel to the substrate because of orthorhombic lattice, the diffraction arc corresponding to both (200) and (110) should be seen at $q = 14.1\ nm^{-1}$ on the equator. This, however, is not the case. Instead, one can predict that the *c*-axis is oriented considerably near the normal of the substrate surface and *a*- and *b*-axes are more or less parallel to the substrate surface. The analysis of GIWAXD data for the MQ and MSC samples is very consistent with the GIRAS data as seen in Fig. 1. Nearly identical GIWAXD characteristics were also observed for 200 nm-thick samples as shown in Fig. 4. But the intensity of arced reflection corresponding to (110)/(200) planes of 200 nm-thick film is stronger than that of 100 nm due to the thickness effect, which is attributed to the fact that thicker sample has higher number of scattering atoms and higher crystallinity than thinner film.

To investigate the effect of ferroelectric-to-paraelectric phase transition on the crystallinity, chain orientation, and dipole orientation in ultra-thin films, 2D-GIWAXD was measured while heating up to 120 °C (above T_c but below T_m) and subsequent cooling down to 30 °C. Curie transition temperature during heating ($T_c^{\uparrow}$) and cooling ($T_c^{\downarrow}$) for the VDF/TrFE (72-28) copolymer were observed to be about 75 °C and 105 °C respectively from the FTIR-GIRAS spectra measured upon heating and cooling for the 70 nm sample [10]. Fig. 5 shows the GIWAXD patterns of the 100 nm-thick P(VDF-TrFE) film on the gold substrate measured during heating up to 120 °C (below T_m) and cooling down to 30 °C Fig. 5a shows the GIWAXD pattern of the AN film at 25 °C. As discussed in Fig. 3, the arced strong reflection corresponding to (110)/(200) planes appears on the meridian. This type of diffraction pattern is maintained at 120 °C. Here, the only difference which is observed in Fig. 5b is that the q_z value at 120 °C is smaller (ca. $q_z = 12.51\ nm^{-1}$) than at 25 °C comparable with Fig. 5a due to the ferroelectric-to-paraelectric phase transition occurring upon heating above the Curie transition temperature ($T_c^{\uparrow}$) [28,29]. This kind of paraelectric diffraction pattern was maintained while cooled down to 80 °C. In general, an electro-inactive paraelectric crystal phase is transformed again into an electro-active ferroelectric crystal phase when it is cooled below the Curie transition temperature ($T_c^{\downarrow}$) for P(VDF-TrFE) with VDF content between 50 and 80%. Meanwhile, the strong arced reflection still remains on the meridian even though the sample is cooled at 39 °C below $T_c^{\downarrow}$ as shown in Fig. 5e. These phenomena reveal that Curie transition does not affect the chain orientation or dipole orientation at all.

To investigate the effect of melting on the changes in chain orientation or dipole orientation, GIWAXD was also measured while heating the sample up to 180 °C (above T_m) and subsequent cooling to 30 °C. Fig. 6 shows GIWAXD patterns of 100 nm-thick P(VDF-TrFE) (72–28) film on the gold substrate measured during heating up to 180 °C above T_m and cooling down to 30 °C. As discussed in previous part, the ferroelectric-to-paraelectric phase transition was observed when the temperature is heated up to the temperature below T_m. The *q* value of the diffraction peak at 140 °C above $T_c^{\uparrow}$ is lowered due to the Curie transition as shown in Fig. 6c and no diffraction peak is observed at 180 °C above the T_m, whereas in Fig. 6e the diffraction peak appears again on the meridian with an additional diffraction peak at the azimuthal angle of 60° due to non-isothermal melt-crystallization into the paraelectric phase having different crystalline orientation from the initial orientation. The *q* values of these two peaks are the same and become higher at lower temperature below $T_c^{\downarrow}$ as shown in Fig. 6f due to the paraelectric-to-ferroelectric phase

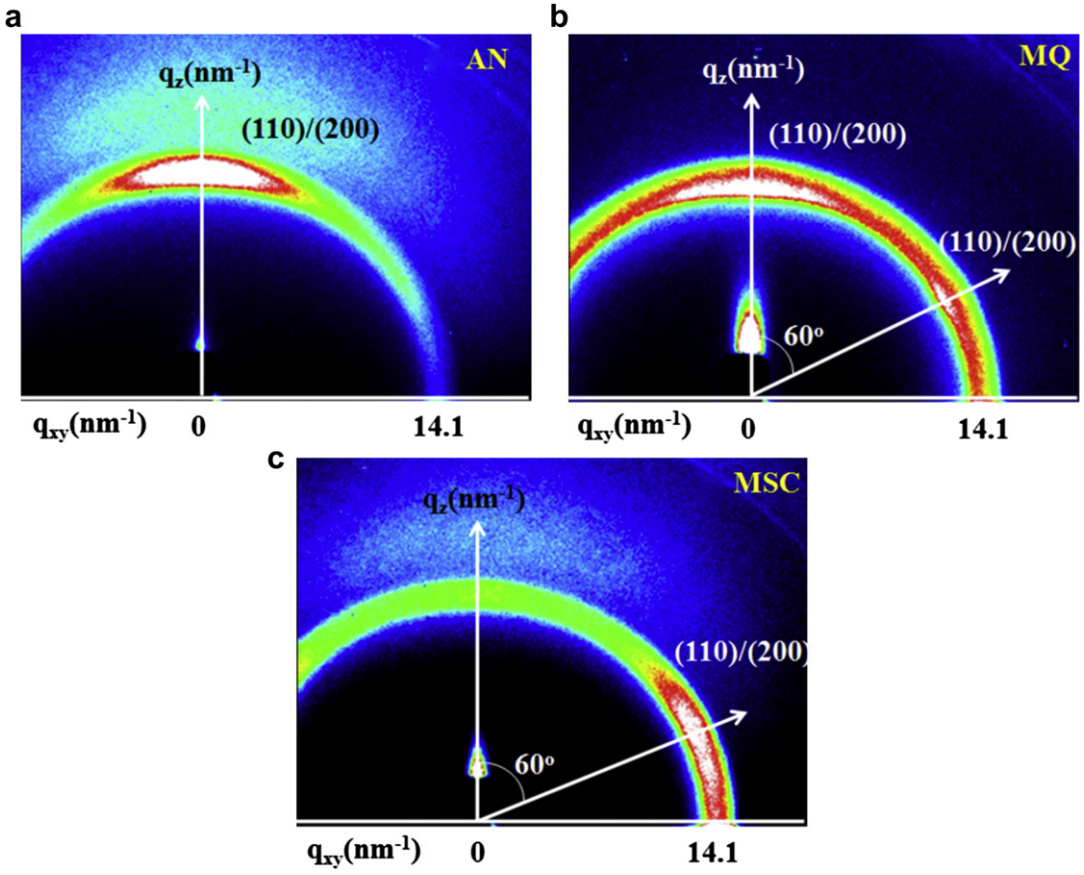

Fig. 4. GIWAXD patterns of the 200 nm-thick P(VDF-TrFE) film spin-cast on the gold substrate with various thermal treatments.

transition. From these experimental results, the effect of melting on changes in chain and dipole orientation is identified. When the temperature is maintained below T_m, the strong arced reflection appeared only on the meridian, whereas the strong arced reflection appeared clearly separated on both meridian and azimuthal angle of 60° upon cooling after melting. This phenomenon can be used by confirming how melting affects changes in the chain and dipole orientations. But, the arced pattern observed on azimuthal angle of 60° appeared weaker than those of MQ and MSC as shown in Fig. 3b,c. This result may be due to the presence of still un-melted initial lamellar crystals of the AN sample as the annealing temperature of 180 °C was not high enough to attain the complete liquid state, compared with the temperature of 200 °C adopted when the MQ and MSC samples were made.

3.3. Surface morphology

From GIRAS and GIWAXD results of P(VDF-TrFE) ultra-thin films prepared with different sample preparation methods, the orientation pattern of lamellar crystal on the surface of ITO or gold substrate could be predicted. Since molecular chains are preferentially oriented along the substrate surface for AC and AN samples, the chain folded lamellar crystals seem to be standing predominantly on their edges, i.e., 'edge-on' lamellar crystal with preferential (200) and (110) contacts with the substrate surface as shown in Fig. 7a. On the contrary, 'face-on' lamellae with their faces on the surface seem to be appropriate for MQ and MSC samples as shown in Fig. 7b, where molecular chains are preferentially oriented near the normal to the substrate surface.

AFM images and histograms of 50 nm-thick P(VDF-TrFE) films subjected to different thermal conditions are shown in Fig. 8. The preparation of the flattest surface with minimum deviation in film thickness to avoid the electrical breakdown has been the main concern. The AC and AN samples shown in Fig. 8a,b exhibit very tiny edge-on crystalline micro domains with short needlelike shape, whose average length and width are only approximately 110 nm and 30 nm, respectively. These two samples also show relatively uniform film thickness as shown in their histograms.

Melt-quenched (MQ) and melt-slowly cooled (MSC) samples exhibited drastically different surface morphology with non-uniform film thickness. The surface morphologies of the MQ and MSC films which underwent non-isothermal crystallization from the melt are shown in Fig. 8c,d. The MQ and MSC samples are seen to have 'face-on' lamellar crystalline domains predominantly as predicted from GIRAS and GIWAXD results. These results are consistent with the previous report [6]. This kind of surface was attributed to the in-plane lamellar structure where the chain axis is oriented preferentially near the normal of the substrate surface as predicted from GIRAS and GIWAXD data. The MQ sample has also a small amount of a very long 'edge-on' lamellar crystal, whose thickness and height are about 140 nm and 25 nm, respectively. Since the average lamellar thickness of common crystalline polymer is 10–12.5 nm, this edge-on lamellar crystal domain appears to consist of a stack of about 12 lamellae. The average thickness of 'face-on' lamellar crystals in Fig. 8d was found to be about 25 nm, which indicates that this 'face-on' lamellar crystal may consist of a stack of two lamellae. The surface topography of 100 nm- (as shown in Fig. 9) and 200 nm-thick samples (not shown here) is also nearly same as that of 50 nm-thick sample for the AC and AN samples, whereas more 'edge-on' lamellar crystals are observed on the 'face-on' lamellae with the increasing film thickness for the MQ and MSC samples. Though the thickness of the lamellar stack can be

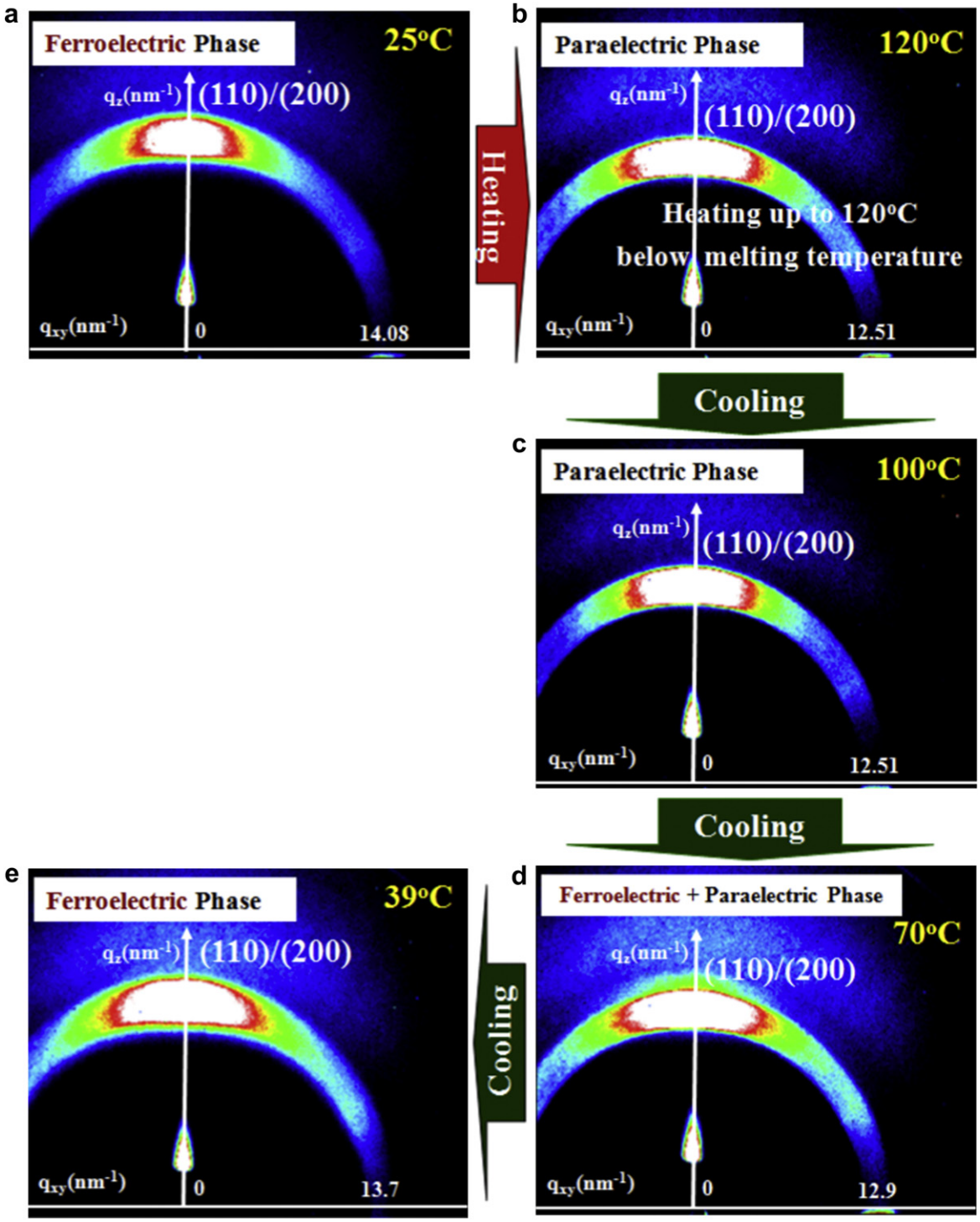

Fig. 5. GIWAXD patterns of the 100 nm-thick P(VDF-TrFE) film on the gold substrate measured during heating up to 120 °C (higher than T_c, butlower than T_m) and cooling down to 30 °C.

measured accurately using SAXS analysis, it should be noted that the surface morphology of each sample prepared with different sample preparation methods is very consistent with the surface morphology predicted from GIRAS and GIWAXD data.

3.4. Change in degree of CF-dipole orientation by poling

When the electric field strength is greater than the coercive field (E_c), CF-dipoles are rotated toward the applied electric field direction. Once the dipoles are switched, they do not return to their initial positions even after removing the electric field. Since this dipole switching process is irreversible until another polarity-opposite electric field larger than the E_c is applied later, the P(VDF-TrFE) films can be a good candidate for NvFePoRAM devices. This irreversible dipole switching results in P_r of the P(VDF-TrFE) copolymer film. The magnitude of P_r is exactly proportional to the resultant degree of CF-dipole orientation toward the poling direction. The CF-dipole realignment of the ultra-thin P(VDF-TrFE) film

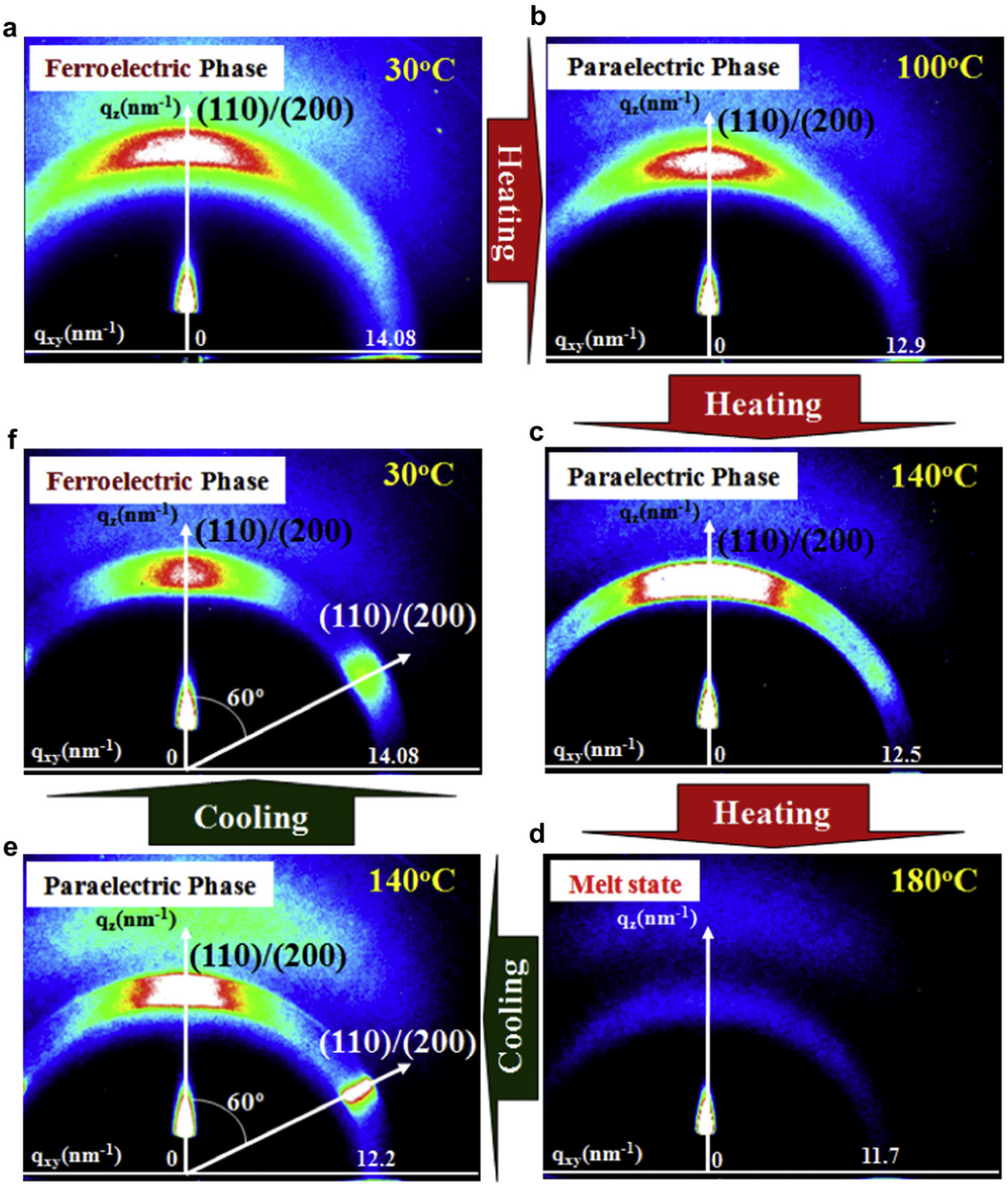

Fig. 6. GIWAXD patterns of the 100 nm-thick P(VDF-TrFE) film on the gold substrate measured during heating up to 180 °C (higher than T_m) and cooling down to 30 °C.

on the gold substrate by poling can also be identified by the GIRAS technique discussed above. The preferentially orientation of the CF-dipoles toward the poling direction through rotating along the chain axis followed by structural reorganization also changes the orientation of *b*- and *a*-axes. As discussed above, GIRAS is very sensitive to changes in the orientation of IR-active vibration moments induced by applying various external stimuli to the ultra-thin polymer film cast on the metal substrate. We measured *in situ* GIRAS spectra for the AN, MQ, and MSC samples during corona poling to see the effect of poling on the CF-dipole orientation. The results are shown in Fig. 10.

For the poled AN sample, every A_1 band whose transition moment is parallel to *b*-axis shows significant increase in IR absorption, whereas every B_2 band whose transition moment is parallel to *a*-axis shows drastic decrease in IR absorbance and B_1 band shows negligibly small absorbance change. This indicates that *b*-axis parallel to CF-dipole is preferentially oriented toward the external electric field direction, in turn this results in the preferential alignment of *a*-axis along the substrate surface but the irreversible CF-rotation along the chain axis does not change the initial *c*-axis orientation. From the intensity ratio of the 888 cm^{-1} peak to the 848 cm^{-1} peak (ca. 0.57:1) after poling and the intrinsic ratio of vibrational transition moment of the 888 cm^{-1} peak to that of the 848 cm^{-1} peak (ca. 1.23:1), the average angles that the transition moment of the 848 cm^{-1} peak, i.e., *b*-axis, and the transition moment of the 888 cm^{-1} peak, i.e., *a*-axis, are making with the

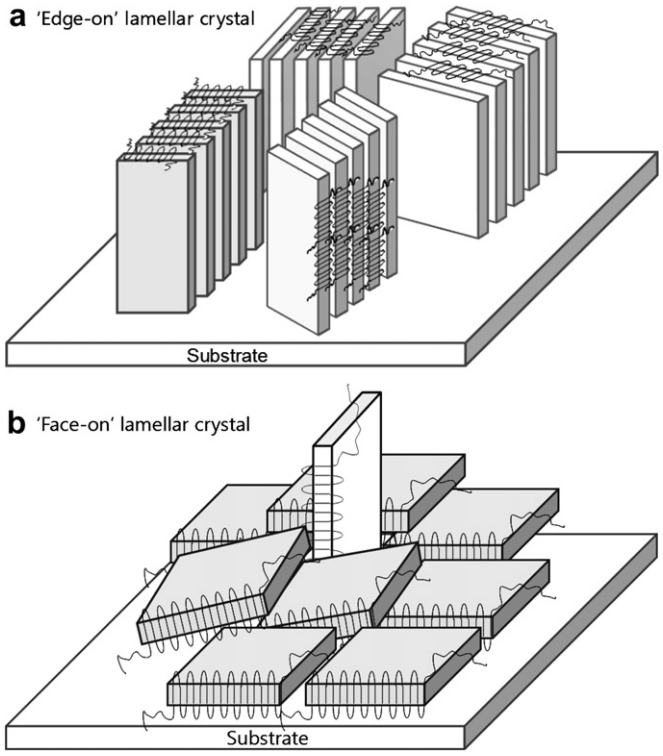

Fig. 7. A schematic diagram of the microstructure based on GIRAS and GIWAXD data. (a) 'edge-on' lamellar crystal; (b) 'face-on' lamellar crystal.

external electric field direction could be calculated to be 58.5° and 31.5°, respectively, using the following relation equation; $1.23^2 \times \cos^2\alpha : 1^2 \times \cos^2\beta = 0.57:1$, where α and β are the angles which *a*-axis and *b*-axis are making with the poling electric field direction (nearly identical to the electric vector of *p*-polarization incident IR beam for the grazing incidence geometry) respectively and $\alpha + \beta = 90°$ due to orthorhombic lattice. In earlier section, the combination of GIWAXD and GIRAS data for the AN sample before poling indicates that the AN sample has mixed (200) and (110) contacts. This big change in α and β after poling, however, can also change the relative contribution of each (200) and (110) contact. Since $\alpha = 58.5°$ is very close to 60° and $\beta = 31.5°$ is very close to 30° after poling, the (110) contact becomes highly predominant through structural reorganization through the irreversible CF-dipole rotation upon poling.

For the MQ and MSC samples, changes in peak intensity of A_1 and B_2 bands are relatively small after poling, when compared with the AN sample. This is because the MQ and MSC samples crystallized non-isothermally crystallized from the melt have more or less preferential orientation of molecular axis near the normal to the substrate surface rather than along the substrate surface, and in turn, the polar *b*-axis aligned preferentially parallel to the substrate becomes very inactive for the CF-dipole rotation toward the poling electric field applied perpendicular to the substrate. The MSC sample is seen to be more inactive to the poling electric field than the MQ sample. This is very consistent with results predicted from the GIRAS data shown in Figs. 1 and 2 and GIWAXD data shown in Figs. 3 and 4.

3.5. P-E hysteresis

Even though the AN sample has a preferential orientation of molecular chain with *c*-axis along the substrate surface, both *a*- and *b*-axes can rotate around the *c*-axis freely under an external electric field as discussed in the previous section. Thus, the external electric field larger than the E_c applied in the poling process and polarization measurement induces the preferential orientation of the polar *b*-axis toward the electric field direction irreversibly, which is responsible for a large permanent polarization of P(VDF-TrFE). This property could be confirmed by measuring the *P-E* hysteresis using Radiant technology Precision LC. For the 50 nm-thick samples, *P-E* hysteresis loops could not be obtained at all probably due to the low crystallinity and frequent electric breakdown caused by pin-hole defect.

Fig. 11a and b show bistable *P-E* hysteresis curves at different external voltage upon bias electric field observed for the 100 nm- and 200 nm-thick AN samples on the ITO-coated glass at 30 °C, respectively. The ferroelectric response is linear at low applied electric field, but shows an apparent switching transient above 0.90–1.0 MV/cm. Saturation phenomenon was observed when electric field higher than 1.9–2.0 MV/cm is applied. The *P-E* curves show asymmetric hysteresis, which may be caused by differences in chemical composition and work function between top (aluminum) and bottom (ITO) electrodes. So the P_r and E_c are obtained from averaging absolute values of $\pm P_r$ and $\pm E_c$, respectively. The P_r is approximately 7.8 μC/cm^2 and the E_c is approximately 0.75 MV/cm for 100 nm-thick film, while the P_r is approximately 6.2 μC/cm^2 and the E_c is approximately 0.80 MV/cm for 200 nm-thick film. After showing saturated polarization response, the E_c did not further increase significantly with increasing applied electric field.

However, when all *c*-axes of lamellar crystals in the P(VDF-TrFE) sample are normal to the substrate surface, i.e., parallel to the electric field, it is impossible to get the preferential orientation of the polar *b*-axis toward the electric field without rotation of the chain molecular *c*-axis requiring extremely high energy in the solid state. Therefore, in this case the P_r becomes zero theoretically. Thus the MQ and MSC samples having more or less orientation of molecular *c*-axis perpendicular to the substrate surface were found to show much reduced peak intensity change for A_1 and B_2 bands of their GIRAS spectra after poling, compared with the AN sample (Fig. 10).

Fig. 11c and d show *P-E* hysteresis loops of the 100 nm- and 200 nm-thick P(VDF-TrFE) films, respectively, on the ITO-coated glass prepared at various thermal conditions as mentioned in the previous section. For the MQ and MSC samples, the P_r is reduced considerably and the E_c is dramatically increased at the nearly same external electric field strength of 2.0 MV/cm, when compared with the AN sample. The considerable reduction in P_r is associated with the reduced amount of 'edge-on' lamellar crystals and the abrupt increase in the E_c is associated with the increased amount of 'face-on' lamellar crystals. These results are very consistent with the prediction from GIRAS spectra after poling as discussed above.

3.6. Nonvolatile memory characteristics via DC-EFM measurement

The ultra-thin ferroelectric polymer film such as P(VDF-TrFE) can be poled by applying a dc bias voltage above the coercive voltage between the probe tip and the conducting substrate (ITO) in dynamic contact scanning along the predetermined areas and lines. The dipole direction after poling can be controlled with the polarity of the applied DC voltage above $\pm E_c$. Poling in this way does not change the surface morphology of the film.

The detection of the poled areas was carried out by measuring the piezoelectric response in the DC-EFM mode on the XE-100 AFM. An ac modulating voltage between the probe tip and the conductive substrate induces the mechanical oscillation normal to the film surface in the poled areas, because the P(VDF-TrFE) is a piezoelectric material. The amplitude of the ac modulating voltage during data reading process must be far below the coercive voltage in order not to change the initial polarization direction. This

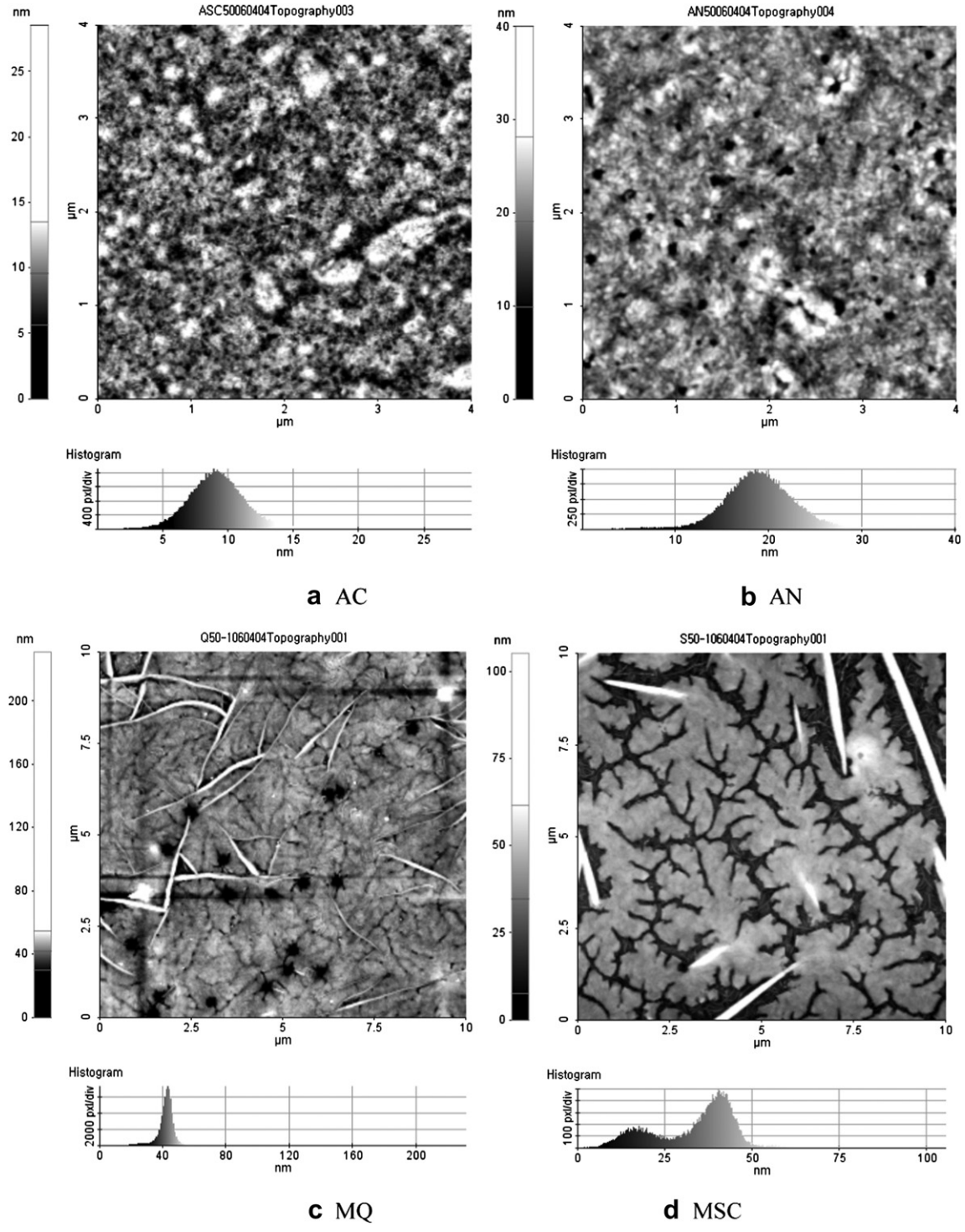

Fig. 8. AFM 2D-topography image (non-contact mode) of the 50 nm-thick P(VDF-TrFE) film as a function of sample preparation condition. Scanned area: 4 μm × 4 μm for (a) and (b); 10 μm × 10 μm for (c) and (d).

piezoelectric vibration amplitude is proportional to the modulating voltage and the P_r and thus the piezoelectric response signal is measured from the cantilever deflection using a lock-in-amplifier. The detected signal is comprised of the amplitude (A) and the phase difference (φ), which correspond to the magnitude and the direction of the polarization in the film, respectively. In this study, $A\cos\varphi$ images with which both magnitude and direction of polarization can be evaluated simultaneously and phase difference images with which the direction of polarization can be only identified were obtained. The frequency and magnitude of the ac modulating peak–peak voltage used for reading a data bit were 17 kHz and 2 V.

Fig. 12 shows topographic and DC-EFM images of 200 nm-thick AN film, obtained simultaneously. Fig. 12a shows the topographic image after writing bit data in an area of 2 × 2 μm^2 within the 4 × 4 μm^2 sample area with a dc bias voltage of −20 V for a duration of 0.5 s per pixel (line pixel density:128 pixels/μm). The written area cannot be identified with a certain level of contrast in a simple topographic image. Instead only small 'edge-on' crystalline grains

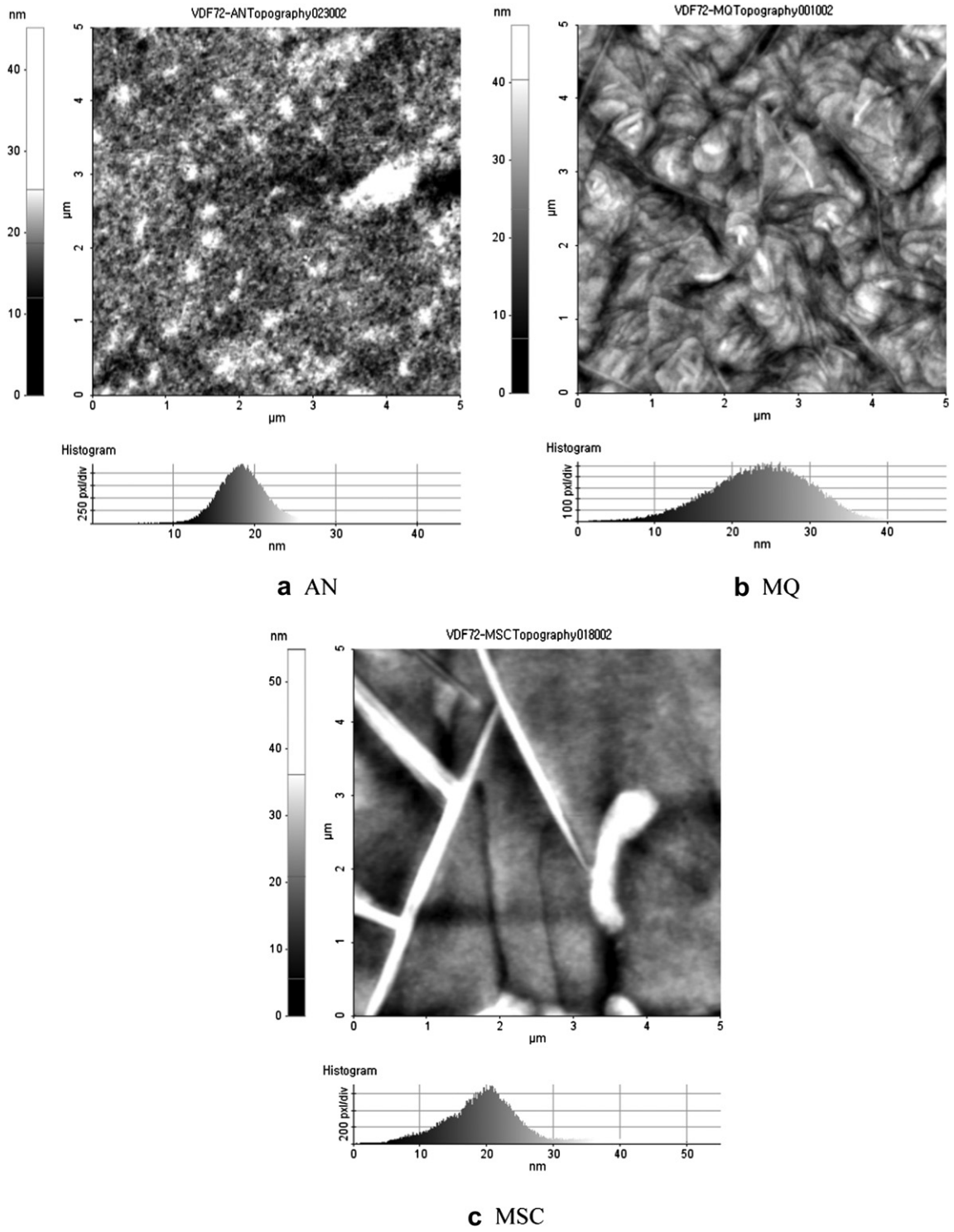

Fig. 9. AFM 2D-topography image (non-contact mode) of the 100 nm-thick film P(VDF-TrFE) as a function of sample preparation condition. Scanned area is 5 μm × 5 μm.

are observed. Fig. 12b,c shows the EFM amplitude and phase images observed in the written area. One can easily distinguish written area from unwritten area with a good contrast in both EFM images due to the difference in total polarization. Fig. 12d shows the topographic image after writing bit data in an area of 4 × 4 μm^2 with a dc bias voltage of −20 V for a duration of 0.5 s per pixel (line pixel density:51 pixels/μm), and then erasing them in an area of 2 × 2 μm^2 inside the previously written area with a dc bias voltage of +20 V for a duration of 0.5 s per pixel. The unwritten, written, and erased areas were not distinguished one another in a simple topographic image either.

Fig. 12e,f shows the EFM amplitude and phase images observed simultaneously in the initially written area (data bit '1') and erased area (data bit '0'). The image contrast of the polarized areas in Fig. 12e,f depends on the magnitude and direction of P_r after poling using the ac modulating voltage of the constant V_{p-p}. The

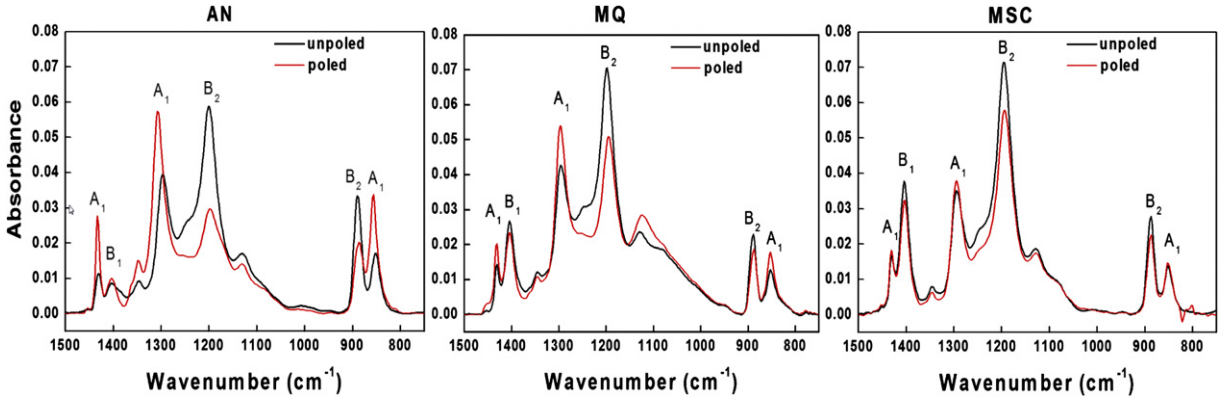

Fig. 10. GIRAS spectra of differently annealed thin films (75 nm) cast on gold-coated Si-wafer before and after corona poling at 16 kV for 30 min.

formation of both domains is caused by the rotation and alignment of electric dipoles within P(VDF-TrFE) molecules along the applied electric fields during writing process. After writing in a $4 \times 4\ \mu m^2$ area, a DC voltage with the opposite polarity was applied in $2 \times 2\ \mu m^2$ area inside the first written area. As a result, the contrast in the amplitude and phase images was reversed, as shown in Fig. 12e,f. This phenomenon is a clear evidence of the polarization reversal of the P(VDF-TrFE) film, which is attributed to the 180° rotation of CF-dipoles along the molecular chains in accordance with the polarity of the applied dc bias.

Since the direction of the pole is clearly discerned, the feasibility of applying the ultra-thin P(VDF-TrFE) film to the SPM-based storage device of WMRM (Write-Many-Read-Many) ability is demonstrated by replacing PMMA film used in the conventional SPM-based storage device of only WORM (Write-Once-Read-Many) ability [30] with the piezoelectric ultra-thin P(VDF-TrFE) film.

The effect of varying tip bias voltages for the 100 nm-thick AN sample is also shown in Fig. 13. With increasing dc bias voltage, topographic image did not change. However, the amplitude and phase images changed depending on the magnitude of the dc bias voltage applied with the same duration time of 500 ms. The formed domain size increased as the magnitude of the bias voltage was increased. The formation of the local domain was much clearer when the magnitude of the bias voltage was above 20 V. It is because this value is much higher than the coercive voltage which was calculated from the piezoelectric hysteresis curve (as shown in Fig. 11).

Fig. 14 shows changes in piezoelectric response images ((a) amplitude and (b) phase) of the 100 nm-thick P(VDF-TrFE) AN

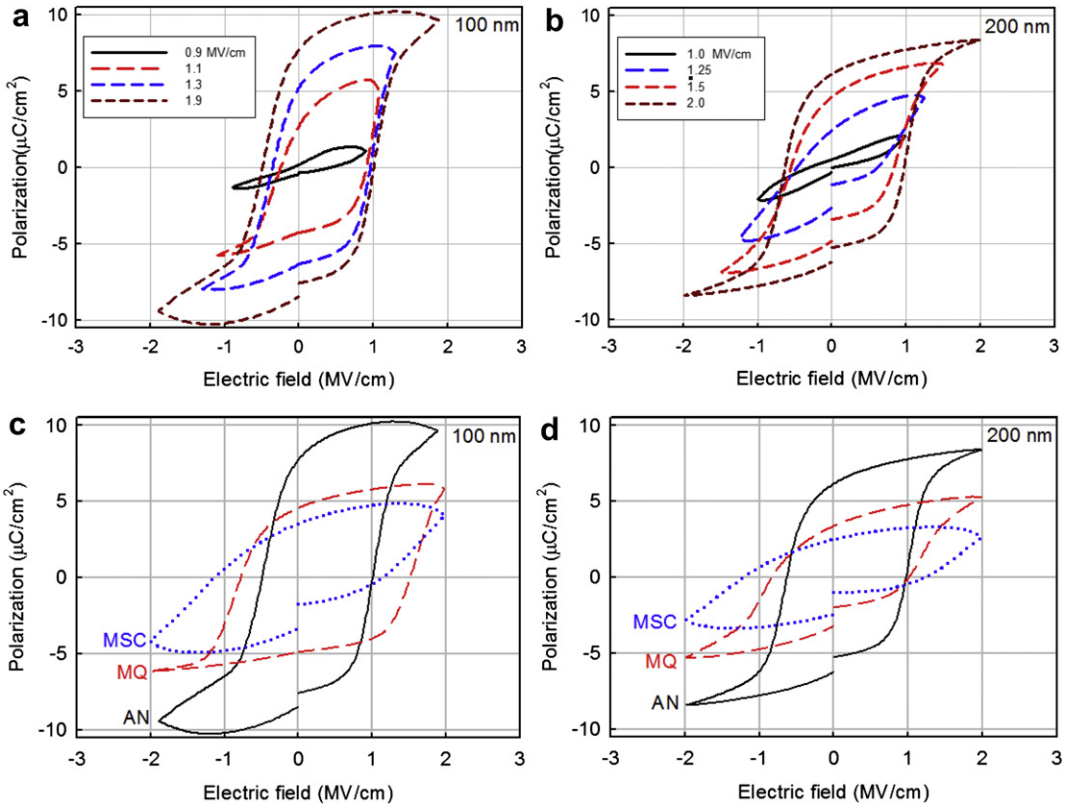

Fig. 11. *P-E* hysteresis curves at different external voltages for (a) 100 nm-thick AN sample; (b) 200 nm-thick AN sample on ITO and changes in *P-E* hysteresis loops with various thermal treatments for (c) 100 nm-thick sample; (d) 200 nm-thick sample.

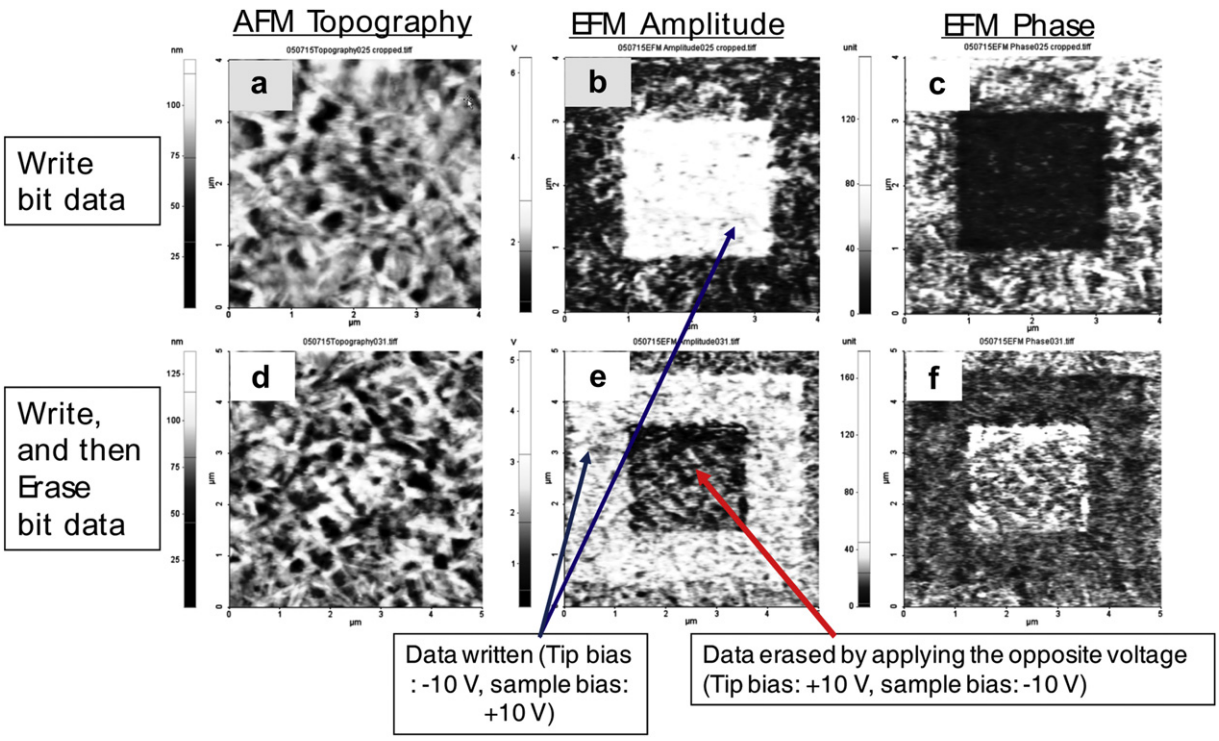

Fig. 12. AFM, DC-EFM amplitude, and DC-EFM phase images for the 200 nm-thick P(VDF-TrFE) AN film on the ITO glass. <Writing only> (a) topographic image after writing bit data in an area of $2 \times 2\ \mu m^2$; (b) EFM amplitude image of (a); (c) EFM phase image of (a); <writing and then erasing> (d) topographic image after writing bit data in an area of $4 \times 4\ \mu m^2$, and then erasing them in an area of $2 \times 2\ \mu m^2$ inside the previously written area; (e) EFM amplitude image of (d); (f) EFM phase image of (d). Writing condition: tip bias voltage = −10 V and sample bias voltage = +10 V; Erasing condition: tip bias voltage = +10 V and sample bias voltage = −10 V.

sample poled with different dc bias applying times. Several local domains with different sizes were formed by applying a dc bias voltage with different durations. The magnitude of the pulse voltages was fixed at 15 V (sample bias voltage = +5 V and tip bias voltage = −10 V). In Fig. 14a, the formation of the local domain could first be detected clearly at the dc applying time of 1 s. The domain size was increased when the dc applying time was increased. The diameter reached more than 200 nm at the dc applying time of above 10 s, and became saturated with the increase of the dc applying time. The diameter of the smallest domain was about 105 nm at the applying time of 1 s. These phenomena show that the domain size in the P(VDF-TrFE) ultra-thin film also strongly depends on the dc applying time. When the dc applying time is too short, the dipoles in the P(VDF-TrFE) molecules cannot be rotated and aligned sufficiently within the direction of the applied electric field. So, no local domains can be clearly detected.

Nanolithography mode in DC-EFM is a technique used to pattern nanoscale data bit on ultra-thin film surface. To demonstrate the writing capability on P(VDF-TrFE) film using DC-EFM, the word

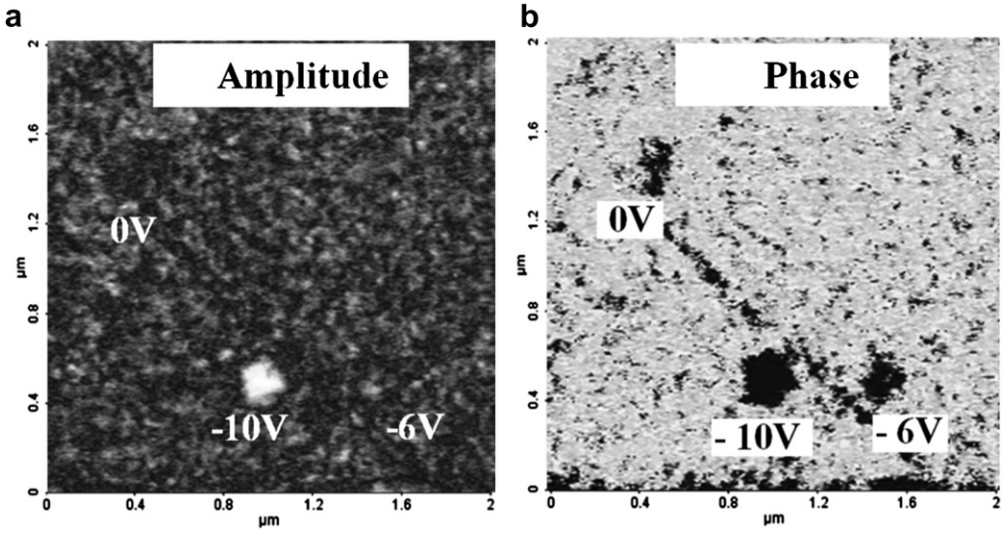

Fig. 13. Effect of tip bias voltage on DC-EFM images of the 100 nm-thick P(VDF/TrFE) AN film. (a) amplitude image and (b) phase image. The magnitude of the sample bias voltages was fixed at +10 V and holding time 500 ms.

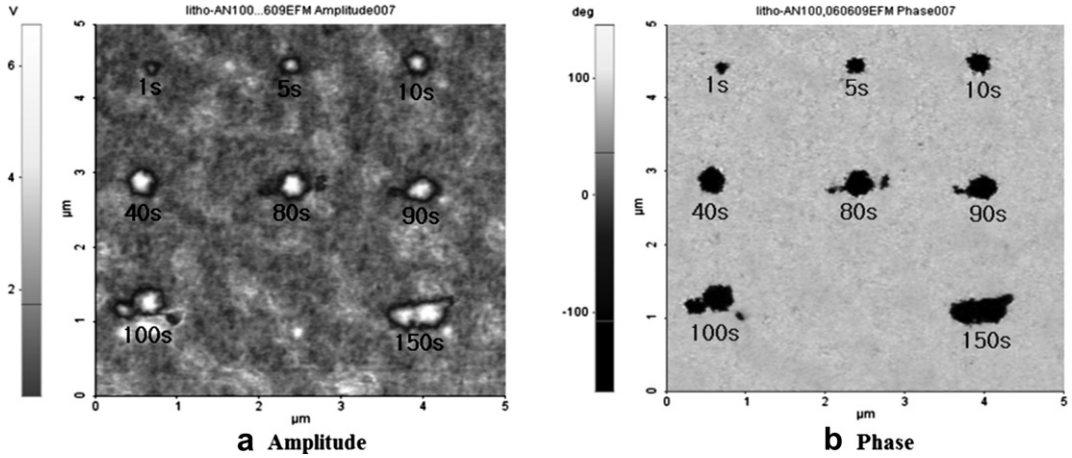

Fig. 14. DC-EFM amplitude and phase images showing the dependence of the domain size in the 100 nm-thick P(VDF-TrFE) AN film on the duration of the pulse voltage with sample bias:+5 V and tip bias:−10 V.

"K H U" and "JongSoonLee" were written on the ultra-thin film in Fig. 15. This figure shows EFM (a) amplitude and (b) phase images obtained simultaneously after writing the characters. Electrical domain of P(VDF-TrFE) film was switched by applying different bias between the tip and sample at different position as shown in Fig. 12. Since the line width of 'K H U' written with very good spatial resolution is about 223 nm, every data bit, 0 or 1, can be recorded at least every square of 500 nm × 500 nm with a high spatial resolution enough to be read. Therefore, as the P(VDF-TrFE) ultra-thin film is used as an SPM-based storage device or a nonvolatile ferroelectric memory device with MFM, MFIS, or FET structure, one can produce a memory device with memory density of about 30 GB/in^2. To increase memory density of the P(VDF-TrFE) ultra-thin film-based memory device, the spatially resolved line width or dot size must be reduced. Since N time reduction of spatially resolved dot size can increase memory density N^2 times, one should devise how to increase the spatial resolution so that one may reduce the size of memory device or maximize the memory capacity of memory device of a limited area. The best way to reduce the size of the unit memory segment for recording or erasing data bit is to reduce the size of the 'edge-on' lamellar crystal without reducing the crystallinity. We will report this method in near future.

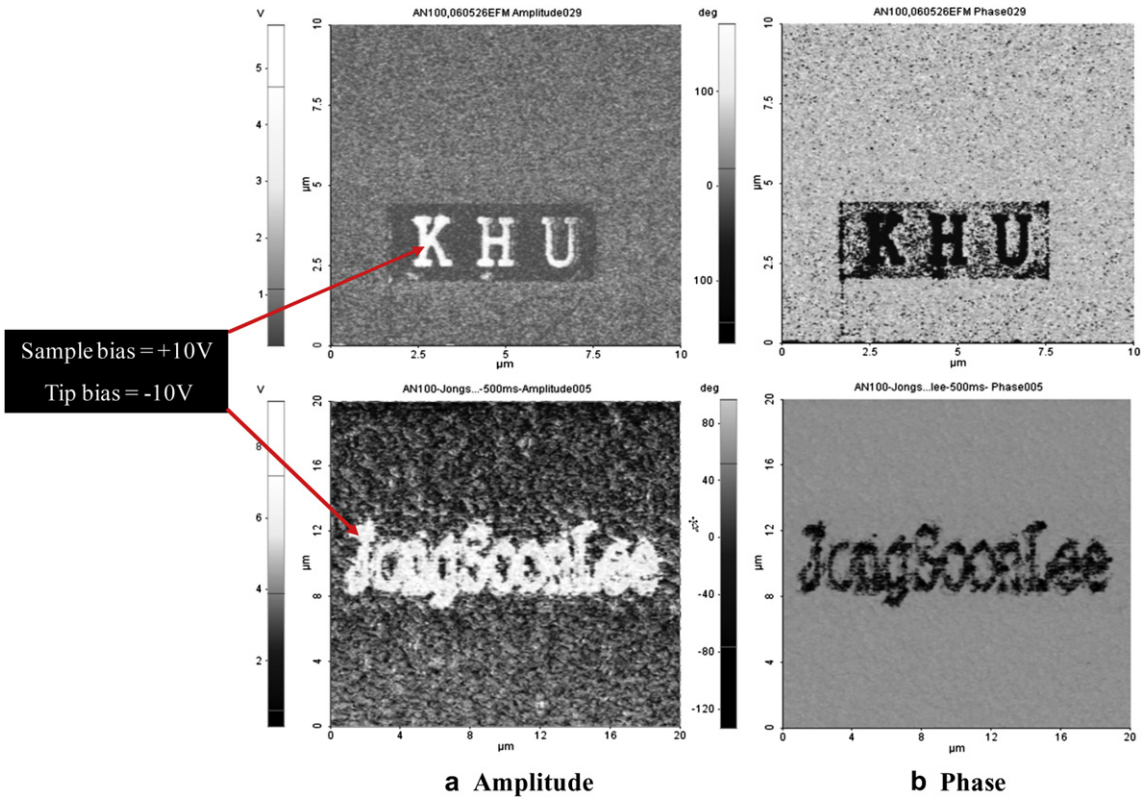

Fig. 15. Ferroelectric patterning examples on the 100 nm-thick P(VDF/TrFE) AN film spin coated on ITO glass substrate sample with a combination of DC-EFM and lithography software. "K H U" is an abbreviation of the authors' affiliation and "JongSoonLee" is the name of the fist author. Sample bias:+10 V and tip bias:−10 V for writing. Reading condition: 2 V at 17 kHz (a) DC-EFM amplitude images; (b) DC-EFM phase images.

4. Conclusions

GIRAS, GIWAXD, and AFM were used extensively in analyzing surface crystalline morphology and chain orientation of ultra-thin ferroelectric P(VDF-TrFE) (72–28) copolymer films prepared with varying thermal histories. For the as-cast (AC) and annealed (AN) samples, most of polymer chains were preferentially oriented along the substrate surface and 'edge-on' lamellar crystals were formed predominantly. On the contrary, melt-crystallized samples (MQ and MSC) show preferential chain orientation near the normal to the surface plane and predominant 'face-on' lamellar crystals. Thus the AN sample showed the largest P_r and the smallest E_c due to the easiest CF_2 dipole rotation by an external electric field, since the AN sample has preferential chain orientation along the conductive substrate surface with higher degree of crystallinity than AC sample. From these phenomena, it could be confirmed that as-cast and then annealing at the temperature (ca. 120 °C) above T_c, but below T_m is the most suitable condition to fabricate the NvFe-PoRAM device when P(VDF-TrFE) is used for the purpose.

DC-EFM technique was successfully used to 'write and erase' the data bit on the ultra-thin P(VDF-TrFE) film by applying a dc bias voltage much larger than coercive voltage with different polarities. And the data bit state could be read by measuring the piezoelectric response of the cantilever with a conductive tip with a lock-in-amplifier by applying an ac modulating voltage whose V_{p-p} is much less than the coercive voltage.

Acknowledgment

This work was supported by Basic Science Research Program through the National Research Foundation of Korea (NRF) funded by the Ministry of Education, Science and Technology (R11-2005-065) and "the National Research Program for the 0.1 Terabit Nonvolatile Memory Development" sponsored by Korea Ministry of Commerce, Industry and Energy.

References

[1] Or SW, Chan HLW, Choy CL. Sensor Actuat A-Phys 2000;80:237.
[2] Wegener M, Gerhard-Multhaupt R. IEEE T Ultrason Ferr 2003;50:921.
[3] Köhler R, Neumann N, Gottfried-Gottfried R. Microelectron Eng 1995; 29:79.
[4] Lee JS, Prabu AA, Chang YM, Kim KJ. Macromol Symp 2007;249–250:13.
[5] Reece TJ, Ducharme S, Sorokin AV, Poulsen M. Appl Phys Lett 2003; 82:142.
[6] Park YJ, Kang SJ, Park C, Kim KJ, Lee HS, Lee MS, et al. Appl Phys Lett 2006;88: 242908.
[7] Bune A, Ducharme S, Fridkin V, Blinov L, Palto S, Petukhova N, et al. Appl Phys Lett 1995;67:3975.
[8] Bune AV, Fridkin VM, Ducharme S, Blinov LM, Palto SP, Sorokin AV, et al. Nature 1998;391:874.
[9] Kim KJ, Reynolds NM, Hsu SL. Macromolecules 1989;22:4395.
[10] Prabu AA, Lee JS, Kim KJ, Lee HS. Vib Spectros 2006;41:1.
[11] Prabu AA, Kim KJ, Park C. Vib Spectros 2009;49:101.
[12] Kim KJ, Hsu SL. Polymer 1994;35:3612.
[13] Naber RCG, Blom PWM, Marsman AW, Leeuw DM. Appl Phys Lett 2004;85: 2032.
[14] Fujisaki S, Ishiwara H, Fujisaki Y. Appl Phys Lett 2007;90:162902.
[15] Noh SH, Choi W, Oh MS, Hwang DK, Lee K, Im S. Appl Phys Lett 2007;90: 253504.
[16] Yamauchi N. Jpn J Appl Phys 1986;25:590.
[17] Lim SH, Rastogi AC, Desu SB. J Appl Phys 2004;96:5673.
[18] Naber RCG, Tanase C, Blom PWM, Gelinck GH, Marsman AW, Touwslager FJ, et al. Nat Mater 2005;4:243.
[19] Gerber A, Kohlstedt H, Fitsilis M, Waser RT, Reece J, Ducharme S, et al. J Appl Phys 2006;100:024110.
[20] Unni KNN, Dabos-Seignon S, Nunzi JM. J Phys D 2005;38:1148.
[21] Gelinck GH, Marsman AW, Touwslager FJ, Setayesh S, de Leeuw DM, Naber RCG, et al. Appl Phys Lett 2005;87:092903.
[22] Xia F, Xu HH, Razavi B, Cheng Z-Y, Zhang QM. J Appl Phys 2002;92:3111.
[23] Park YJ, Kang SJ, Lotz B, Thierry A, Kim KJ, Park C. Macromolecules 2008;41: 109.
[24] Guy IL, Unsworth J. J Appl Phys 1987;61:5374.
[25] Tashiro K, Tanaka R. Polymer 2006;47:5433.
[26] Jin XY, Kim KJ, Lee HS. Polymer 2005;46:12410.
[27] Bellet-Amalric E, Legrand JF. Eur Phys J B 1998;3:225.
[28] Kim KJ, Kim GB, Vanlencia CL, Rabolt JF. J Polym Sci Pol Phys 1994;32:2435.
[29] Kim KJ, Kim GB. Polymer 1997;38:4881.
[30] Yoo IK. Testing and characterization of ferroelectric thin film capacitors. In: Hong SB, editor. Nanoscale phenomena in ferroelectric thin films. Norwell: Kluwer Academic Publishers; 2004 [chapter 1 p. 3].